



# Photoenhanced sulfate formation by the heterogeneous uptake of SO<sub>2</sub> on non-photoactive mineral dust

Wangjin Yang, Jiawei Ma, Hongxing Yang, Fu Li, and Chong Han

School of Metallurgy, Northeastern University, Shenyang, 110819, China

**Correspondence:** Chong Han (hanch@smm.neu.edu.cn)

Received: 12 June 2023 – Discussion started: 20 October 2023

Revised: 7 April 2024 – Accepted: 10 April 2024 – Published: 12 June 2024

**Abstract.** Heterogeneous uptake of SO<sub>2</sub> on mineral dust is a predominant formation pathway of sulfates, whereas the contribution of photo-induced SO<sub>2</sub> oxidation to sulfates on the dust interfaces still remains unclear. Here, we investigated heterogeneous photochemical reactions of SO<sub>2</sub> on five mineral oxides (SiO<sub>2</sub>, kaolinite, Al<sub>2</sub>O<sub>3</sub>, MgO, and CaO) without photocatalytic activity. Light enhanced the uptake of SO<sub>2</sub>, and its enhancement effects negatively depended on the basicity of mineral oxides. The initial uptake coefficient ( $\gamma_{0,BET}$ ) and the steady-state uptake coefficient ( $\gamma_{s,BET}$ ) of SO<sub>2</sub> positively relied on light intensity, relative humidity (RH), and O<sub>2</sub> content, while they exhibited a negative relationship with the initial SO<sub>2</sub> concentration. Rapid sulfate formation during photo-induced heterogeneous reactions of SO<sub>2</sub> with all mineral oxides was confirmed to be ubiquitous, and H<sub>2</sub>O and O<sub>2</sub> played key roles in the conversion of SO<sub>2</sub> to sulfates. In particular, triplet states of SO<sub>2</sub> (<sup>3</sup>SO<sub>2</sub>) were suggested to be the trigger for photochemical sulfate formation. Atmospheric implications supported a potential contribution of interfacial SO<sub>2</sub> photochemistry on non-photoactive mineral dust to atmospheric sulfate sources.

## 1 Introduction

As an important trace gas in the atmosphere, SO<sub>2</sub> is mainly emitted by volcanic eruption and fuel combustion. There is an uneven distribution of atmospheric SO<sub>2</sub> concentrations that show a distinctive seasonal and regional differentiation. Typical mixing ratios of SO<sub>2</sub> in the troposphere are below 0.5 ppb for clean-weather days, rising to several hundred parts per billion during polluted days in urban regions (Ma et al., 2020). About half of SO<sub>2</sub> is oxidized to sulfates (He et al., 2012), which are key components of fine particulates in the atmosphere. High sulfate loading in PM<sub>2.5</sub> was observed (Shao et al., 2019), especially in polluted regions where high-sulfur fuels are usually used (Olson et al., 2021). They significantly alter physicochemical properties of aerosols in terms of hygroscopicity, acidity, and light absorption (Chan and Chan, 2003; Cao et al., 2013; Lim et al., 2018). Sulfates may lead to negative health outcomes, such as respiratory illnesses and cardiovascular diseases (Shiraiwa et al., 2017). In addition, the deposition of sulfates leads to adverse effects on ecosystems via the acidification of soils and lakes

(Golobokova et al., 2020). Therefore, the oxidation of SO<sub>2</sub> to form sulfates has attracted widespread attention in the past decades.

The conversion of SO<sub>2</sub> to sulfates in the atmosphere usually occurs in different phases: gas-phase oxidation of SO<sub>2</sub> by hydroxyl radicals ( $\bullet$ OH) or Criegee intermediate radicals (Mauldin et al., 2012; Davis et al., 1979); aqueous-phase reactions of SO<sub>2</sub> with O<sub>3</sub>, peroxides, or transition metal ions dissolved in cloud and fog droplets (Alexander et al., 2009; Herrmann et al., 2000; Harris et al., 2013; Liu et al., 2020; Li et al., 2020); and heterogeneous SO<sub>2</sub> uptake on aerosols, including authentic mineral dust, soot, inorganic ion, and organic compounds (Adams et al., 2005; G. He et al., 2018; Ye et al., 2018; S. Wang et al., 2019; Yao et al., 2019; R. Zhang et al., 2020; Liu et al., 2020, 2021). However, the oxidation of SO<sub>2</sub> in gas and aqueous phases fails to explain high sulfate concentrations in polluted areas. Model simulation suggests that the rapid sulfate formation can be attributed to heterogeneous SO<sub>2</sub> uptake (Li et al., 2017). A positive relationship between the fraction of sulfates and mineral dust in haze days has been reported, implying that mineral dust may ac-

count for the formation of sulfates (J. Wang et al., 2020). Moreover, large numbers of sulfates were observed on the surface of mineral dust after long-distance transport (Prospero, 1999). Thus, investigating the heterogeneous oxidation of SO<sub>2</sub> on mineral dust can provide basic data for the model calculation to evaluate atmospheric sulfates.

Mineral dust, as the dominant component of particulate matters in the atmosphere, accounts for about 30 %–60 % mass fractions of global aerosols (Dentener et al., 1996; Peng et al., 2012). It primarily contains SiO<sub>2</sub> (40 %–80 %), followed by Al<sub>2</sub>O<sub>3</sub> (10 %–15 %), Fe<sub>2</sub>O<sub>3</sub> (6 %–13 %), CaO (3 %–10 %), MgO (1 %–7 %), and TiO<sub>2</sub> (0.1 %–5 %) (Urupina et al., 2019, 2021; Usher et al., 2003). Mineral dust can provide active sites for the adsorption and reaction of gases. Up to now, the heterogeneous SO<sub>2</sub> uptake on authentic mineral aerosols and model mineral oxides has been widely reported (Ma et al., 2019; Goodman et al., 2001; T. Wang et al., 2018, 2020), with the uptake coefficient ( $\gamma$ ) of SO<sub>2</sub> varying from 10<sup>−9</sup> to 10<sup>−4</sup> (Urupina et al., 2019; Usher et al., 2002).

It was recognized that light could significantly enhance the heterogeneous conversion of SO<sub>2</sub> to sulfates on the surface of photocatalytic mineral dust (Chen et al., 2021; Li et al., 2019; T. Wang et al., 2020). Electron–hole pairs are produced via photo-induced electrons from the valence band to the conduction band of photocatalytic metal oxides and then react with H<sub>2</sub>O and O<sub>2</sub> to generate reactive oxygen species (ROS) such as •OH and •O<sub>2</sub><sup>−</sup> (Chu et al., 2019). Sulfates are produced by the heterogeneous reactions of SO<sub>2</sub> with ROS (Park and Jang, 2016; Park et al., 2017; Langhammer et al., 2020; Bounechada et al., 2017). In particular, due to the large abundance of non-photoactive mineral dust (more than 85 % mass of total mineral dust in the atmosphere) (Usher et al., 2003; Liu et al., 2022), revealing the photooxidation processes of SO<sub>2</sub> on these mineral dust is of great importance to better reevaluate the sulfate formation on aerosols at a global scale.

Photochemical SO<sub>2</sub> uptake and sulfate formation on non-photoactive mineral oxides were investigated using a flow reactor and in situ diffuse reflectance infrared Fourier transform spectroscopy (DRIFTS). The conversion of SO<sub>2</sub> to sulfates was examined under various conditions, and the roles of light intensity, SO<sub>2</sub> concentration, H<sub>2</sub>O, O<sub>2</sub>, and basicity of mineral oxides were determined. Reaction mechanisms and atmospheric implications were proposed, highlighting an important pathway accounting for the photochemical uptake of SO<sub>2</sub> to form sulfates on the non-photoactive surfaces.

## 2 Experimental methods

### 2.1 Materials

Analytical-grade SiO<sub>2</sub> (Sinopharm Chemical Reagent Co., Ltd.), kaolinite (Sinopharm Chemical Reagent Co., Ltd.), Al<sub>2</sub>O<sub>3</sub> (Alfa Aesar), MgO (Sigma-Aldrich), and CaO (Sigma-Aldrich) were used in the experiments. Through

the nitrogen Brunauer–Emmett–Teller (BET) physisorption analysis, their specific surface areas were detected to be 0.419, 6.407, 8.137, 10.948, and 6.944 m<sup>2</sup> g<sup>−1</sup>, respectively. With BaSO<sub>4</sub> used as the reference, the ultraviolet–visible (UV-vis) light absorption spectra of samples (Fig. S1 in the Supplement) in the wavelength range of 300–800 nm were obtained by the Shimadzu UV-2550 spectrophotometer, which was equipped with a diffuse-reflection integrating sphere attachment. The solid powder (0.2–5 g) was uniformly dispersed into 10.0 mL ethanol solution. The mixed liquid was poured into a rectangular quartz sample dish (14.0 cm × 7.0 cm) and dried to form a solid coating in an oven at 353 K for 10 h. SO<sub>2</sub> standard gas (50 ppm in N<sub>2</sub>, Shenyang Air Liquide Co., Ltd.) and high-purity N<sub>2</sub> and O<sub>2</sub> (99.999 vol.%, Shenyang Air Liquide Co., Ltd.) were used as received. The solid sample powder (0.2 g) was immersed in 10 mL deionized water (20 mg mL<sup>−1</sup>), and then the suspension was vigorously stirred for 10 min. The pH of SiO<sub>2</sub>, kaolinite, Al<sub>2</sub>O<sub>3</sub>, MgO, and CaO suspension was measured to be 6.27, 6.58, 9.33, 10.61, and 12.72, respectively, using a pH meter.

### 2.2 Rectangular flow reactor

The uptake experiments of SO<sub>2</sub> on mineral dust were performed in a horizontal rectangular flow reactor (26.0 cm length × 7.5 cm width × 2.0 cm height), which is depicted in Fig. S2. In a previous study, a similar rectangular flow reactor was designed, and the feasibility of the reactor has been verified (Knopf et al., 2007). The reactor was made of quartz to allow the transmission of light. The temperature was maintained at 298 K by circulating temperature-controlled water through the outer jacket of the reactor. Synthetic air with a N<sub>2</sub>/O<sub>2</sub> volume ratio of 4 : 1 was introduced into the flow reactor, and its total flow rate was 1000 mL min<sup>−1</sup>. The Reynolds number ( $Re$ ) was calculated to be 28.2 ( $Re < 200$ ), as described in the Supplement, indicating a laminar flow state. SO<sub>2</sub>, together with high-purity N<sub>2</sub> (100 mL min<sup>−1</sup>), was introduced into the reactor through a movable T-shaped injector equipped with six exit holes (0.2 mm diameter) so that the gas could be uniformly distributed over the width of the reactor. The SO<sub>2</sub> concentration was 40–200 ppb and measured with a SO<sub>2</sub> analyzer (Thermo 43i). Wet N<sub>2</sub> generated with a bubbler containing deionized water was introduced by two parallel inlets on the side of a T-shaped injector. Relative humidity (RH, 10 %–75 %) was controlled by regulating the ratio of dry N<sub>2</sub> to wet N<sub>2</sub> and measured via a hygrometer (Center 314). The equivalent layer numbers of water on the surface were 0.9–4.0, according to the Brunauer–Emmett–Teller (BET) model (Sumner et al., 2004), and the thickness of the film of adsorbed water varied between 2.7–12 nm at RH = 10 %–75 %. There were three equally spaced exhaust ports to mitigate the outlet turbulence. A xenon lamp (CEL-LAX500, China Education Au-light Co., Ltd.) was used to simulate sunlight and vertically located above the reactor. A

filter was placed on the reactor to remove the light with wavelengths shorter than 300 nm. The spectrum irradiance of the xenon lamp is displayed in Fig. S3 and was measured using a calibrated spectroradiometer (ULS2048CL-EVO, Avantes). The spectral irradiance was measured inside the reactor after passing the water cooling and in the absence of a sample. The total irradiance ( $0\text{--}7.93 \times 10^{16}$  photons  $\text{cm}^{-2} \text{s}^{-1}$ ) on the coating can be adjusted by varying the distance of the xenon lamp to the reactor.

### 2.3 Uptake coefficient of SO<sub>2</sub>

The heterogeneous reaction kinetics of SO<sub>2</sub> with mineral dust can be described by a pseudo-first-order reaction. Figure S4 shows a linear relationship between the natural logarithm of the SO<sub>2</sub> concentration and the reaction time. The apparent rate constant ( $k_{\text{obs, SiO}_2}$ ) of SO<sub>2</sub> with SiO<sub>2</sub> can be calculated using Eq. (1),

$$\frac{\ln(C_0/C_1)}{t} = k_{\text{obs, SiO}_2}, \quad (1)$$

where  $C_0$  and  $C_1$  (ppb) are the initial SO<sub>2</sub> concentration and the SO<sub>2</sub> concentration at the exposure time  $t$ , respectively;  $t$  was calculated by dividing the length of the reactive surface by the average flow velocity. The loss of SO<sub>2</sub> on the internal wall of the reactor in blank experiments was carried out under various conditions (Fig. S5 as an example), and it has been deducted for the  $\gamma$  calculation. Assuming that the wall loss was constant in the experiments with and without samples, the geometric uptake coefficient ( $\gamma_{\text{geo}}$ ) was determined by Eq. (2) (Knopf et al., 2007),

$$\gamma_{\text{geo}} = \frac{4Vk}{S\omega}, \quad (2)$$

where  $k$  ( $\text{s}^{-1}$ ),  $V$  ( $4 \times 10^{-4} \text{ m}^3$ ),  $S$  ( $9.8 \times 10^{-3} \text{ m}^2$ ), and  $\omega$  ( $314.05 \text{ m s}^{-1}$ ) are the reaction rate constant, the volume of the rectangular reactor, the surface area of the sample dish, and the mean molecular speed of SO<sub>2</sub>, respectively.

The uptake process of SO<sub>2</sub> on SiO<sub>2</sub> depended on the reaction of SO<sub>2</sub> with SiO<sub>2</sub> and the mass transport of SO<sub>2</sub> to the surface. It can be expressed by Eq. (3),

$$k'_{\text{r, SiO}_2} = \left[ \frac{1}{k_{\text{obs, SiO}_2} - k_{\text{obs, wall}}} - \frac{a}{NuD} \right]^{-1}, \quad (3)$$

where  $k_{\text{obs, SiO}_2}$  and  $k_{\text{obs, wall}}$  ( $\text{s}^{-1}$ ) are the apparent rate constants measured with and without SiO<sub>2</sub> samples, respectively.  $k'_{\text{r, SiO}_2}$  is the reaction rate constant of SO<sub>2</sub> accounting for the diffusion effect;  $D$  ( $0.1337 \text{ cm}^2 \text{ s}^{-1}$ ) is the diffusion coefficient of SO<sub>2</sub> in air;  $a$  (1 cm) is one-half the height of the flow reactor; and  $Nu$  represents the Nusselt numbers obtained with a calculation method from Solbrig and Gidaspow (1967), which represents the mass transport. The corrected  $\gamma$  can be calculated by Eq. (2), where  $k$  was replaced by  $k'_{\text{r, SiO}_2}$ . In our

experiments, the correction for  $\gamma$  was estimated to be 10 %. Initial uptake coefficients ( $\gamma_0$ ) and steady-state uptake coefficients ( $\gamma_s$ ) were calculated by averaging the signals within the 1.0 and 40–60 min reaction time, respectively.

To understand the diffusion depth of SO<sub>2</sub> and determine the interaction of SO<sub>2</sub> with the underlying layers of SiO<sub>2</sub>, the uptake of SO<sub>2</sub> as a function of the SiO<sub>2</sub> mass under irradiation is shown in Fig. S6. The  $\gamma$  exhibited a linear increase in the SiO<sub>2</sub> mass range of 0.05–2.0 g, while it remained unchanged at the SiO<sub>2</sub> mass > 3.0 g. Therefore, the uptake coefficient of SO<sub>2</sub> in the linear regions was normalized using the BET surface area of SiO<sub>2</sub> by Eq. (4) (Brunauer et al., 1938),

$$\gamma_{\text{BET}} = \frac{S_{\text{geo}} \times \gamma_{\text{geo}}}{S_{\text{BET}} \times m_{\text{SiO}_2}}, \quad (4)$$

where  $\gamma_{\text{BET}}$  is the SO<sub>2</sub> uptake coefficient normalized to the BET surface area,  $S_{\text{geo}}$  ( $9.8 \times 10^{-3} \text{ m}^2$ ) is the geometric area of the sample dish,  $S_{\text{BET}}$  ( $0.419 \text{ m}^2 \text{ g}^{-1}$ ) is the BET surface area of SiO<sub>2</sub>, and  $m_{\text{SiO}_2}$  (0.05–2.0 g) is the SiO<sub>2</sub> mass. The same method was also used to calculate the uptake coefficients of SO<sub>2</sub> on other mineral oxides.

### 2.4 In situ DRIFTS analysis

The changes in the chemical compositions on mineral oxides in the SO<sub>2</sub> uptake process were investigated by a Fourier transform infrared (FTIR) spectrometer (Thermo Nicolet iS50) equipped with an in situ diffuse reflectance accessory and a mercury cadmium telluride (MCT) detector. About 14 mg of mineral oxides was placed into a stainless-steel cup inside the reaction cell. To remove adsorbed impurities, SiO<sub>2</sub> was purged with a  $150 \text{ mL min}^{-1}$  airflow (N<sub>2</sub>/O<sub>2</sub> volume ratio = 4 : 1) at RH = 40 % for 1 h. Then, a background spectrum of unreacted samples was collected. SO<sub>2</sub> (2 ppm) was introduced into the reaction cell, and the IR spectra were recorded as a function of time at a resolution of  $4 \text{ cm}^{-1}$  by averaging 100 scans. The light from the xenon lamp (500 W) was transmitted into the DRIFTS reaction cell via a fiber. To verify the role of intermediates, Ru(bpy)<sub>3</sub>(Cl)<sub>2</sub> and NaHCO<sub>3</sub>, acting as <sup>3</sup>SO<sub>2</sub> and •OH scavengers (Bulgakov and Safonova, 1996; Gen et al., 2019a), respectively, were mixed with SiO<sub>2</sub> powder in an agate mortar, and the mixture was put in the reaction cell of DRIFTS.

## 3 Results and discussion

### 3.1 Photoenhanced uptake of SO<sub>2</sub>

Acting as the most abundant of the mineral oxides, SiO<sub>2</sub> was used to investigate the uptake behaviors of SO<sub>2</sub>. As shown in Fig. 1a, when SO<sub>2</sub> (80 ppb) was exposed to SiO<sub>2</sub> in the dark, the SO<sub>2</sub> concentration decreased to 70 ppb, and then it quickly increased and reached a steady state after 20 min.

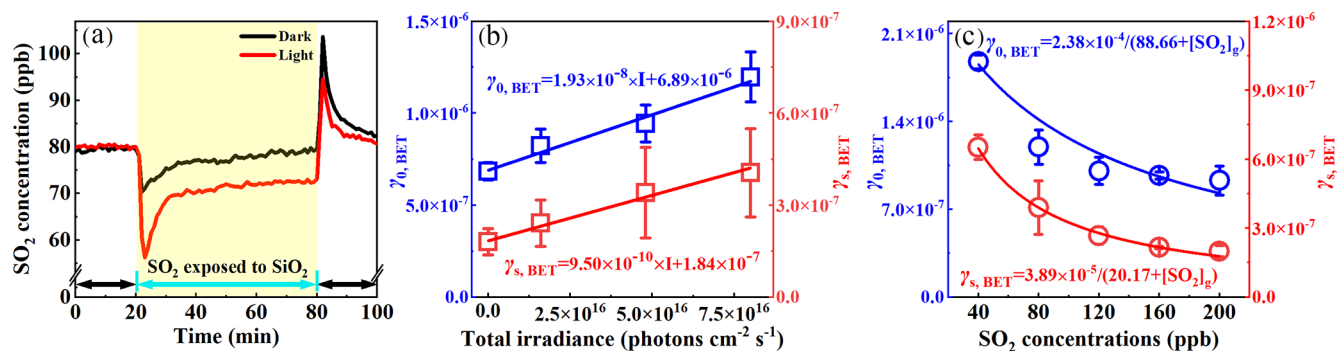


**Figure 1.** (a) The temporal variation in the SO<sub>2</sub> concentration on SiO<sub>2</sub> in the dark and under irradiation ( $7.93 \times 10^{16}$  photons cm<sup>-2</sup> s<sup>-1</sup>); the background changes in the SO<sub>2</sub> concentration in the blank reactor have been deducted. (b) The  $\gamma_{0,BET}$  and  $\gamma_{s,BET}$  of SO<sub>2</sub> on SiO<sub>2</sub> as a function of the light intensity. (c) The  $\gamma_{0,BET}$  and  $\gamma_{s,BET}$  of SO<sub>2</sub> on SiO<sub>2</sub> at different SO<sub>2</sub> concentrations under irradiation ( $7.93 \times 10^{16}$  photons cm<sup>-2</sup> s<sup>-1</sup>). The fitting lines for  $\gamma_{0,BET}$  and  $\gamma_{s,BET}$  were based on the Langmuir–Hinshelwood mechanism using Eq. (6). Reaction conditions: SiO<sub>2</sub> mass of 0.2 g, temperature of 298 K, RH of 40 %, and O<sub>2</sub> content of 20 %.

Upon exposure to SiO<sub>2</sub> under irradiation, the SO<sub>2</sub> concentration exhibited a greater drop than that in the dark. The deactivation of SO<sub>2</sub> uptake on SiO<sub>2</sub> was very slight after 20 min under irradiation. These results suggest that light can promote the heterogeneous reaction of SO<sub>2</sub> on SiO<sub>2</sub>. Few studies have observed the photochemical uptake of SO<sub>2</sub> on non-photoactive minerals (Xu et al., 2021; Zhang et al., 2022). When SO<sub>2</sub> did not come into contact with SiO<sub>2</sub>, its concentration recovered rapidly. The desorption of SO<sub>2</sub> was observed when SO<sub>2</sub> was isolated from SiO<sub>2</sub> in the dark and under irradiation, indicating that the physical adsorption partially contributed to the SO<sub>2</sub> loss during the photochemical process. The proportion of the desorbed SO<sub>2</sub> during the uptake process can be quantified by dividing the integral of reversible desorption of SO<sub>2</sub> ( $t = 80$ – $100$  min) into the integral of the SO<sub>2</sub> uptake ( $t = 20$ – $80$  min), which was calculated to be 95 % and 12 % in the dark and under irradiation, respectively. This implies that SO<sub>2</sub> uptake in the dark was primarily ascribed to the physical adsorption of SO<sub>2</sub>, while SO<sub>2</sub> uptake under irradiation was mainly attributed to chemical processes or irreversible adsorption.

The uptake coefficients of SO<sub>2</sub> on SiO<sub>2</sub> as a function of irradiation intensity are shown in Fig. 1b. The errors in all figures are the standard deviations of three repetitive experiments. Both  $\gamma_{0,BET}$  and  $\gamma_{s,BET}$  displayed a strong linear relationship with the irradiation intensity. The  $\gamma_{0,BET}$  and  $\gamma_{s,BET}$  under the irradiation of  $7.93 \times 10^{16}$  photons cm<sup>-2</sup> s<sup>-1</sup> were 1.75 and 2.25 times those in the dark, respectively. This further confirms the photochemical nature of the reactions of SO<sub>2</sub> on SiO<sub>2</sub>. In particular,  $\gamma_{0,BET}$  and  $\gamma_{s,BET}$  on SiO<sub>2</sub> under simulated solar irradiation were comparable with those ( $10^{-7}$ – $10^{-6}$ ) on Gobi Desert dust (GDD) and Arizona test dust (ATD) under UV irradiation, which contained photocatalytic metal oxides (Park et al., 2017). As for the SO<sub>2</sub> uptake on TiO<sub>2</sub>,  $\gamma_{0,BET}$  and  $\gamma_{s,BET}$  were measured to be  $10^{-6}$  and  $10^{-7}$ , respectively, using the flow tube (Ma et al., 2019),

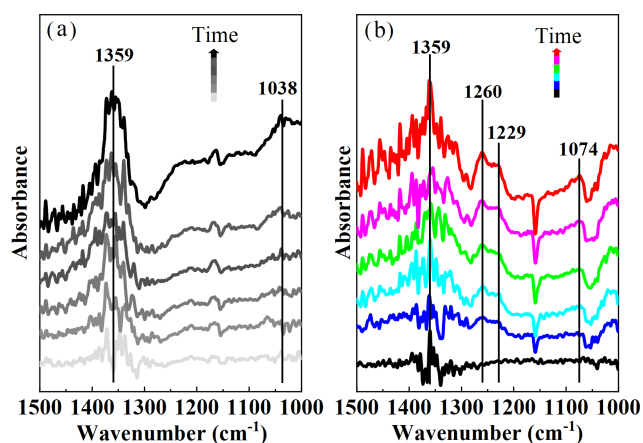
which were similar to our results. It should be pointed out that the similar uptake coefficient did not mean the comparable ability of photoactive and non-photoactive mineral oxides to SO<sub>2</sub> uptake, since the uptake coefficient was highly dependent on environmental conditions (SO<sub>2</sub> concentration, relative humidity, mineral oxides mass, light source, and pressure) and reactor type (chamber and flow tube reactor). Table S1 in the Supplement shows that the percentage of SiO<sub>2</sub> in the sample was 99.02 %, accompanied by a small amount of Al<sub>2</sub>O<sub>3</sub>, K<sub>2</sub>O, Fe<sub>2</sub>O<sub>3</sub>, and CaO. Photoactive substances (Fe<sub>2</sub>O<sub>3</sub>) were very few in the sample, and they should not be the main contributor to the photochemical uptake of SO<sub>2</sub>.

Figure 1c shows the evolution of  $\gamma_{0,BET}$  and  $\gamma_{s,BET}$  at different SO<sub>2</sub> concentrations under irradiation. An inverse dependence of  $\gamma_{0,BET}$  and  $\gamma_{s,BET}$  on the SO<sub>2</sub> concentration was observed, meaning that the efficiency of SO<sub>2</sub> uptake decreased with increasing the SO<sub>2</sub> concentration. The uptake of gases on the solid surfaces usually follows the Langmuir–Hinshelwood (L–H) mechanism (Ammann et al., 2003; T. Zhang et al., 2020), suggesting that gaseous molecules are quickly absorbed on the surfaces, and then the reactions occur among the absorbed species. Assuming that the adsorption of SO<sub>2</sub> on SiO<sub>2</sub> is in accordance with the Langmuir isotherm, the dependence of  $\gamma$  on the SO<sub>2</sub> concentration can be described by Eq. (5) (T. Zhang et al., 2020):

$$\gamma = \frac{(4V/S\omega)k[\text{SiO}_2]_{\text{T}}K_{\text{SO}_2}}{1 + K_{\text{SO}_2}[\text{SO}_2]_{\text{g}}}, \quad (5)$$

where [SO<sub>2</sub>]<sub>g</sub> is the concentration of gaseous SO<sub>2</sub>, [SiO<sub>2</sub>]<sub>T</sub> is the total number of active sites on SiO<sub>2</sub>,  $k$  is the reaction rate constant of SO<sub>2</sub> absorbed on SiO<sub>2</sub>, and  $K_{\text{SO}_2}$  represents the Langmuir adsorption constant of SO<sub>2</sub>. Because the SiO<sub>2</sub> mass remained constant during the reaction, Eq. (5) can be written as Eq. (6):





**Figure 2.** In situ DRIFTS spectra of SiO<sub>2</sub> during the uptake process of SO<sub>2</sub> (2 ppm) in the dark (a) and under irradiation (b). Reaction conditions: RH of 40 %, temperature of 298 K, and O<sub>2</sub> content of 20 %.

$$\gamma = \frac{a}{1 + K_{\text{SO}_2}[\text{SO}_2]_{\text{g}}}, \quad (6)$$

where  $a = (4V/S\omega)k[\text{SiO}_2]K_{\text{SO}_2}$ . As shown in Fig. 1c, Eq. (6) can well describe the correlation of the SO<sub>2</sub> uptake coefficient with the SO<sub>2</sub> concentration, suggesting that the L–H mechanism can explain the influence of the SO<sub>2</sub> concentration on  $\gamma_{0,\text{BET}}$  and  $\gamma_{\text{s,BET}}$ .

### 3.2 Photo-induced formation of sulfates by the SO<sub>2</sub> uptake

To investigate the products formed on SiO<sub>2</sub>, in situ DRIFTS spectra were recorded, as shown in Fig. 2. The band at 1359 cm<sup>-1</sup> was assigned to physically adsorbed SO<sub>2</sub> on SiO<sub>2</sub> (Urupina et al., 2019). The bidentate sulfates and bisulfates contributed to the bands at 1260 and 1229/1074 cm<sup>-1</sup> (Urupina et al., 2019; Yang et al., 2020), respectively. The band at 1038 cm<sup>-1</sup> may be related to the monodentate sulfites (Yang et al., 2019; Z. Wang et al., 2019). It was noted that the intensity of physically adsorbed SO<sub>2</sub> (1359 cm<sup>-1</sup>) under irradiation was lower than that in the dark (Fig. S7), which may be ascribed to further conversion of SO<sub>2</sub> adsorbed on SiO<sub>2</sub> under irradiation. The sulfate bands in particular (1260, 1229, and 1074 cm<sup>-1</sup>) only appeared under irradiation, while the sulfites (1038 cm<sup>-1</sup>) were only detected in the dark. This suggests that light changed the SO<sub>2</sub> conversion pathways on SiO<sub>2</sub>. As shown in Fig. S7, the bands at 1157/1055 cm<sup>-1</sup> were assigned to the asymmetric stretching of Si–O (Hu et al., 2003). Sulfates generated on the surface may interact with SiO<sub>2</sub>, leading to a decrease in the intensity of peaks (1157/1055 cm<sup>-1</sup>).

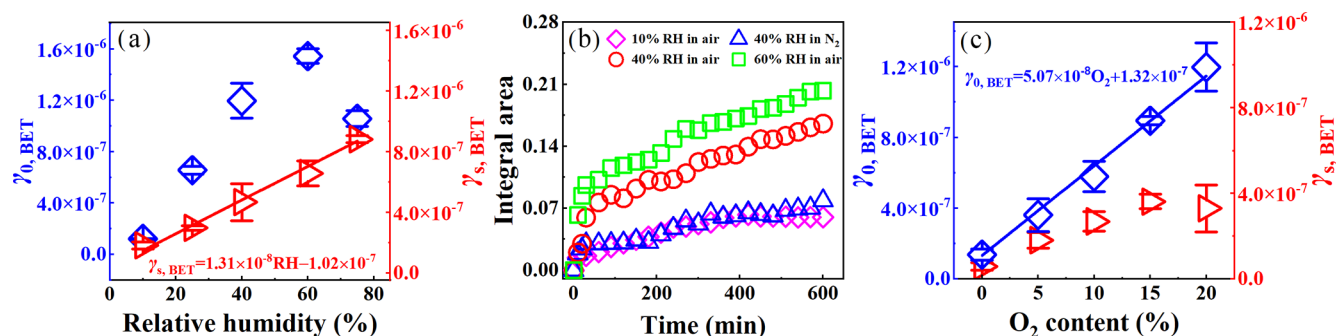
### 3.3 Key roles of H<sub>2</sub>O and O<sub>2</sub> in photochemical conversion of SO<sub>2</sub> to sulfates

Figure S8a shows temporal variations in the SO<sub>2</sub> concentration in the reaction with SiO<sub>2</sub> at RH = 10 % and 60 % under irradiation. The uptake of SO<sub>2</sub> was very weak at RH = 10 %, whereas it was obvious at RH = 60 %. Moreover, H<sub>2</sub>O prolonged the time to reach the steady-state uptake of SO<sub>2</sub>. This means that H<sub>2</sub>O plays an enhancement role in the photochemical uptake of SO<sub>2</sub>. As shown in Fig. 3a,  $\gamma_{0,\text{BET}}$  had a continuous increase from  $(1.20 \pm 0.04) \times 10^{-7}$  to  $(1.54 \pm 0.07) \times 10^{-6}$  with increasing the RH in the 10 %–60 % range, but it decreased to  $(1.05 \pm 0.09) \times 10^{-6}$  at RH = 75 %. The  $\gamma_{\text{s,BET}}$  linearly depended on the RH, and linear fitting to  $\gamma_{\text{s,BET}}$  versus RH yielded an equation  $\gamma_{\text{s,BET}} = 1.31 \times 10^{-8} \times \text{RH} - 1.02 \times 10^{-7}$ . Adsorbed H<sub>2</sub>O promoted the hydration and dissociation of SO<sub>2</sub> (Huang et al., 2015), and it may generate reactive oxygen species (ROS) such as •OH or HO<sub>2</sub> radicals to oxidize SO<sub>2</sub> under irradiation (Li et al., 2020; Ma et al., 2019), which would lead to positive effects of RH on the SO<sub>2</sub> uptake. Adsorbed H<sub>2</sub>O also occupied adsorptive and active sites on the surface, leading to a decrease in SO<sub>2</sub> adsorption. When this competitive role was dominant, the uptake of SO<sub>2</sub> was hindered.

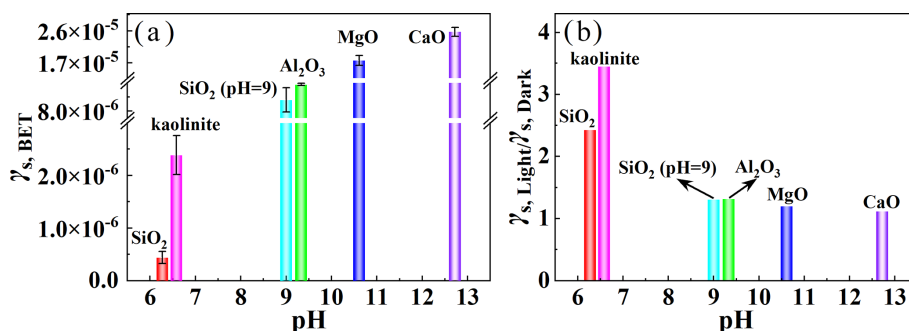
The DRIFTS spectra of SiO<sub>2</sub> during the SO<sub>2</sub> uptake at different RHs are shown in Fig. S9a. The band intensities of sulfates (1260 and 1229 cm<sup>-1</sup>) at RH = 60 % were stronger than those at RH = 10 %, suggesting that H<sub>2</sub>O promotes the sulfate formation. To further investigate the influence of H<sub>2</sub>O on the sulfate formation, the integrated area of sulfates in the DRIFTS spectra (1289–1202 cm<sup>-1</sup>) as a function of the time at different RHs is illustrated in Fig. 3b. Sulfates exhibited a fast formation in the initial 30 min, and then they were continuously generated at a relatively slow rate. SO<sub>2</sub> absorption on the surface was blocked because of the accumulation of H<sub>2</sub>O and products (sulfites and sulfates), resulting in the gradual deactivation of the surface. It was noted that sulfate formation was more prominent at higher RHs, revealing that H<sub>2</sub>O can act as an important participator in the production of sulfates by the photochemical uptake of SO<sub>2</sub> on SiO<sub>2</sub>.

Figure S8b displays effects of O<sub>2</sub> on the photochemical uptake of SO<sub>2</sub> on SiO<sub>2</sub>. Negligible SO<sub>2</sub> uptake occurred in N<sub>2</sub>, while there was a significant decrease in the SO<sub>2</sub> concentration in air. The  $\gamma_{0,\text{BET}}$  greatly increased from  $(1.37 \pm 0.45) \times 10^{-7}$  under anaerobic conditions to  $(1.19 \pm 0.13) \times 10^{-6}$  under 20 % O<sub>2</sub> content conditions (Fig. 3c), confirming that O<sub>2</sub> was involved in the reaction of SO<sub>2</sub> on SiO<sub>2</sub>. The  $\gamma_{\text{s,BET}}$  increased from  $(7.10 \pm 2.85) \times 10^{-8}$  under anaerobic conditions to  $(4.37 \pm 0.58) \times 10^{-7}$  under 15 % O<sub>2</sub> content conditions, whereas it remained unchanged with O<sub>2</sub> content further increasing.

DRIFTS spectra of SiO<sub>2</sub> during the SO<sub>2</sub> uptake in N<sub>2</sub> and air were compared in Fig. S9b. In both air and N<sub>2</sub>, the bands of adsorbed SO<sub>2</sub> were 1359 cm<sup>-1</sup> and those of sulfates were



**Figure 3.** (a) The dependence of  $\gamma_{0,BET}$  and  $\gamma_{s,BET}$  on RH. (b) Integrated area of sulfates in DRIFTS spectra ( $1289\text{--}1202\text{ cm}^{-1}$ ) as a function of time. (c) The dependence of  $\gamma_{0,BET}$  and  $\gamma_{s,BET}$  on O<sub>2</sub>. Reaction conditions: SiO<sub>2</sub> mass of 0.2 g, irradiation intensity of  $7.93 \times 10^{16}$  photons  $\text{cm}^{-2}\text{ s}^{-1}$ , temperature of 298 K, O<sub>2</sub> content of 20 % for (a), and RH of 40 % for (b).



**Figure 4.** (a) The dependence of  $\gamma_{s,BET}$  under irradiation on the basicity (pH) of mineral oxides. (b) The ratios of steady-state uptake coefficients under irradiation to those in the dark ( $\gamma_{s,Light}/\gamma_{s,Dark}$ ). Reaction conditions: mineral oxides mass of 0.2 g, irradiation intensity of  $7.93 \times 10^{16}$  photons  $\text{cm}^{-2}\text{ s}^{-1}$ , temperature of 298 K, RH of 40 %, and O<sub>2</sub> content of 20 %.

$1260$ ,  $1229$ , and  $1074\text{ cm}^{-1}$ . Nevertheless, their intensities in N<sub>2</sub> were weaker than those in air. According to the integrated area of sulfates in the DRIFTS spectra ( $1289\text{--}1202\text{ cm}^{-1}$ ), the formation trends of sulfates were similar in N<sub>2</sub> and air (Fig. 3b), while the sulfate formation rate in N<sub>2</sub> was obviously lower than that in air, meaning that O<sub>2</sub> enhanced the sulfate production. It was reported that the production rate of sulfates from the SO<sub>2</sub> uptake on TiO<sub>2</sub> and by the photolysis of nitrates under UV irradiation in N<sub>2</sub> was also smaller than that in air (Ma et al., 2019; Gen et al., 2019b). In addition, it was noted that sulfates can be generated in N<sub>2</sub>, meaning that O<sub>2</sub> was not necessary and some pathways contributed to sulfates without O<sub>2</sub>.

### 3.4 Ubiquitously photoenhanced conversion of SO<sub>2</sub> to sulfates

To better assess the potential for photochemical conversion of SO<sub>2</sub> to sulfates, the SO<sub>2</sub> uptake experiments were further performed on typical mineral oxides without photocatalytic activity. As displayed in Fig. S10, more obvious SO<sub>2</sub> uptake on kaolinite, Al<sub>2</sub>O<sub>3</sub>, MgO, and CaO was observed under irradiation compared to that in the dark. Figure 4a shows that there was the largest  $\gamma_{s,BET}$  for CaO among five minerals, and

$\gamma_{s,BET}$  positively depended on the basicity (pH) of mineral oxides. Basic oxides generally contain more surface hydroxyls, which enhance the heterogeneous uptake of SO<sub>2</sub> (Zhang et al., 2006). The ratios of steady-state uptake coefficients under irradiation to those in the dark ( $\gamma_{s,Light}/\gamma_{s,Dark}$ ) were larger than 1.0 for all mineral oxides (Fig. 4b). The experiments for the pH dependence on SiO<sub>2</sub> have also been performed (Fig. S11). The pH of SiO<sub>2</sub> suspension was adjusted to pH = 9, and  $\gamma_{s,BET}$  and  $\gamma_{s,Light}/\gamma_{s,Dark}$  were determined to be  $(8.79 \pm 0.85) \times 10^{-6}$  and 1.31, respectively (Fig. 4a and b). These results suggest that light can generally enhance the SO<sub>2</sub> uptake on minerals at a wide pH range. However, the  $\gamma_{s,Light}/\gamma_{s,Dark}$  had smaller values with an increase in the basicity, suggesting that the promotion effect of the light was less remarkable for basic oxides.

As shown in Fig. 5a and b, the band at  $1300\text{ cm}^{-1}$  should be ascribed to the sulfates. The intensity of sulfates ( $1300$  and  $1220\text{ cm}^{-1}$ ) under irradiation was larger than those in the dark. Compared to weaker peaks of sulfates ( $1200$  and  $1260\text{ cm}^{-1}$ ) for Al<sub>2</sub>O<sub>3</sub> in the dark (Fig. 5c), a stronger band of bisulfates appeared at  $1220\text{ cm}^{-1}$  under irradiation (Fig. 5d). In contrast to the generation of sulfates for kaolinite and Al<sub>2</sub>O<sub>3</sub>, both sulfite and sulfate formations were ob-

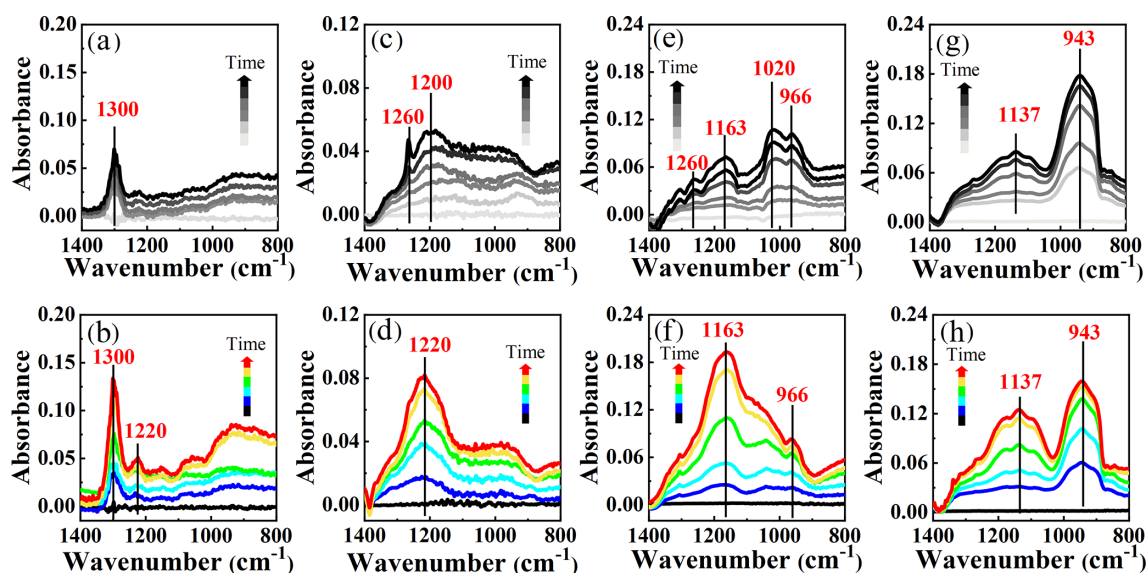


**Figure 5.** In situ DRIFTS spectra of kaolinite (a, b), Al<sub>2</sub>O<sub>3</sub> (c, d), MgO (e, f), and CaO (g, h) during the uptake process of SO<sub>2</sub> (2 ppm) for 600 min in the dark (black lines) and under irradiation (colorful lines). Reaction conditions: RH of 40 %, temperature of 298 K, and O<sub>2</sub> content of 20 %.

served for MgO and CaO (Fig. 5e–h). Sulfites were dominant in the dark, as shown by the peaks at 966 and 1020 cm<sup>-1</sup> for MgO and 943 cm<sup>-1</sup> for CaO, whereas the sulfate formation was significantly enhanced under irradiation according to peak intensities at 1163 cm<sup>-1</sup> for MgO and 1137 cm<sup>-1</sup> for CaO. It should be noted that these mineral oxides were non-photoactive because of their poor light absorption properties (Fig. S1). Nevertheless, the light can promote the formation of sulfates via the SO<sub>2</sub> uptake process on mineral oxides without photocatalytic activity.

### 3.5 Conversion mechanisms of SO<sub>2</sub> to sulfates

Heterogeneous photochemical reaction mechanisms of SO<sub>2</sub> on non-photoactive mineral dust were proposed in light of experimental observations (Fig. 6). Gaseous SO<sub>2</sub> was adsorbed on the surface (R1) and then reacted with H<sub>2</sub>O to form sulfites (R2). Under irradiation, adsorbed SO<sub>2</sub> accepted photons to form its singlet states (<sup>1</sup>SO<sub>2</sub>) and <sup>3</sup>SO<sub>2</sub> (R3–R5) (Sidebottom et al., 1972; Martins-Costa et al., 2018). The reaction between <sup>3</sup>SO<sub>2</sub> and H<sub>2</sub>O resulted in the formation of HOSO• and •OH (R6), which can combine with SO<sub>2</sub> to produce HOSO<sub>2</sub>• (R7). HOSO• and HOSO<sub>2</sub>• can be transformed into SO<sub>3</sub>, which reacted with H<sub>2</sub>O to drive the sulfate formation (R8 and R9). The interaction between <sup>3</sup>SO<sub>2</sub> and O<sub>2</sub> may also generate SO<sub>3</sub> directly, which would be subsequently converted to sulfates (R10). Theoretical calculations suggested that the multistep reactions between <sup>3</sup>SO<sub>2</sub> with H<sub>2</sub>O and O<sub>2</sub> had small energy barriers or were barrier-free (Gong et al., 2022), which could enhance the generation of ROS and the transformation of S(IV) to S(VI). As displayed by R11 and R12, SO<sub>2</sub> and H<sub>2</sub>SO<sub>3</sub> adsorbed on the surface

may be oxidized to form sulfates via the reactions with ROS, including •O, •OH, or HO<sub>2</sub>•, which were produced in R6 and R8–R10. In addition, gaseous SO<sub>2</sub> could be dissolved into adsorbed H<sub>2</sub>O to generate bisulfites, which would be finally converted to sulfates by ROS (R13) (Urupina et al., 2019). As displayed in Fig. S12a, the IR peaks of sulfates were not observed when tris(2,2′-bipyridine)ruthenium dihydrochloride (Ru(bpy)<sub>3</sub>(Cl)<sub>2</sub>) was employed as the quencher of <sup>3</sup>SO<sub>2</sub>. The peaks were assigned to the vibrations of excited Ru(bpy)<sub>3</sub>(Cl)<sub>2</sub> (Mukuta et al., 2014). This definitely proves that <sup>3</sup>SO<sub>2</sub> is the key trigger for the sulfate formation. Figure S12b shows that the peaks of sulfates were weaker in the presence of NaHCO<sub>3</sub>, confirming the dominant contribution of •OH formed in R6 and R9 to the formation of sulfates.

Several photochemical mechanisms have been reported to explain the sulfate formation via the SO<sub>2</sub> uptake on various surfaces. Photoactive mineral oxides (such as TiO<sub>2</sub>, F<sub>2</sub>O<sub>3</sub>, and ZnO) can accept photons to produce electron–hole pairs, which generated ROS for the conversion of SO<sub>2</sub> to sulfates (Ma et al., 2019; Li et al., 2019; T. Wang et al., 2020). For example, •OH and HO<sub>2</sub>•, generated from the reaction of the hole with H<sub>2</sub>O and the electron with O<sub>2</sub>, respectively, can act as oxidizing agents for the reaction with SO<sub>2</sub> (Ma et al., 2019). Similarly, the reaction of SO<sub>2</sub> with photo-induced •OH obviously enhanced the formation of sulfates on diesel soot and actual PM<sub>2.5</sub> (Zhang et al., 2022; Y. Zhang et al., 2020). NO<sub>2</sub> and NO<sub>2</sub><sup>-</sup>/HNO<sub>2</sub> can be formed in the nitrates photolysis and primarily contribute to the oxidation of SO<sub>2</sub> to sulfates on nitrates (Gen et al., 2019b, a). Theoretically, the mechanism proposed in this study should also occur on photo-excited substrates. Taking TiO<sub>2</sub> as an example, SO<sub>2</sub> competed with TiO<sub>2</sub> for photons, and the production effi-

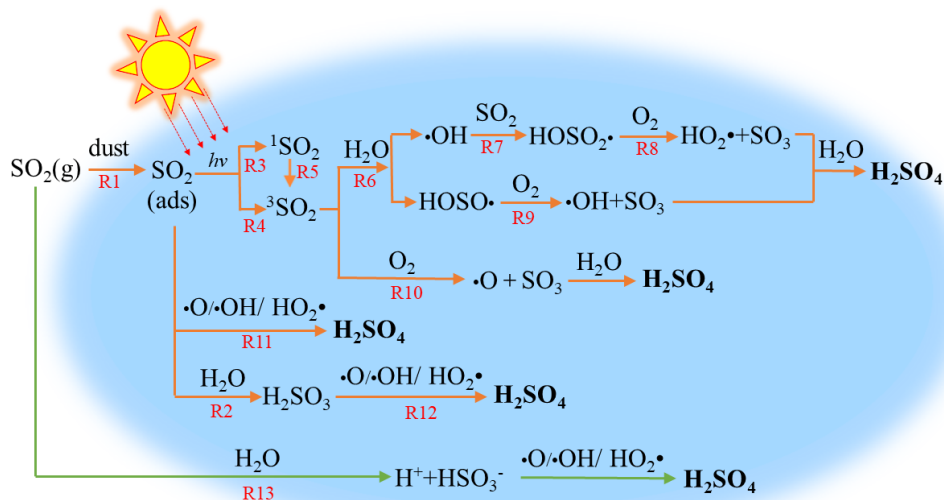


**Figure 6.** The proposed photochemical conversion mechanisms of SO<sub>2</sub> to sulfates on non-photoactive mineral dust.

ciency of <sup>3</sup>SO<sub>2</sub> and excited state of TiO<sub>2</sub> (TiO<sub>2</sub><sup>\*</sup>) depended on their light absorption properties. Meanwhile, <sup>3</sup>SO<sub>2</sub> has competition with electron–hole pairs generated from TiO<sub>2</sub><sup>\*</sup> for O<sub>2</sub> and H<sub>2</sub>O. Thus, the dominant mechanism for the SO<sub>2</sub> uptake on TiO<sub>2</sub> should be related to light absorption properties of precursors and the reactivity for <sup>3</sup>SO<sub>2</sub> and TiO<sub>2</sub><sup>\*</sup> to O<sub>2</sub> and H<sub>2</sub>O. By contrast, all mineral oxides used here cannot be excited under irradiation according to their light absorption spectra (Fig. S1). Nevertheless, SO<sub>2</sub> adsorbed on mineral oxides can absorb ultraviolet radiation (290–400 nm) to form the excited states of SO<sub>2</sub> (SO<sub>2</sub><sup>\*</sup>) (Kroll et al., 2018), which subsequently reacted with H<sub>2</sub>O and O<sub>2</sub>, finally converting SO<sub>2</sub> to sulfates. The SO<sub>2</sub> uptake experiment in the dark and the visible light (> 420 nm) was carried out (Fig. S13). An ignorable difference was observed for the SO<sub>2</sub> concentration with or without visible light, suggesting that visible light had a minor contribution to the photoenhanced SO<sub>2</sub> uptake.

According to the experimental results, some surfaces providing absorptive sites for SO<sub>2</sub> can enhance the photooxidation of SO<sub>2</sub> to sulfates. However, the promotion effect would vary with different substances. For example, the current experiments on some basic minerals indicate that light plays a minor enhancement role in the SO<sub>2</sub> uptake (Fig. 4), but it could still enhance the sulfate formation (Fig. 5). The solubility and effective Henry's law constant of SO<sub>2</sub> were positively dependent on pH. Thus, SO<sub>2</sub> was more liable to be dissolved to form HSO<sub>3</sub><sup>-</sup>/SO<sub>3</sub><sup>2-</sup> on a more alkaline surface, leading to a strong SO<sub>2</sub> uptake in the dark (Fig. 4a and b) and abundant sulfites on surfaces (Fig. 5). Nevertheless, gaseous SO<sub>2</sub> tends to be adsorbed on kaolinite and Al<sub>2</sub>O<sub>3</sub> due to less solubility of SO<sub>2</sub> on these surfaces, and then it is converted to sulfates under irradiation (Fig. 6). Accordingly, a promotion effect

of light on SO<sub>2</sub> uptake was observed on neutral and weakly alkaline surfaces (Fig. 4b).

#### 4 Atmospheric implications

The lifetime ( $\tau$ ) for photochemical loss of SO<sub>2</sub> on mineral dust was given using Eq. (7),

$$\tau = \frac{4}{\gamma\omega A}, \quad (7)$$

where  $\gamma$  and  $\omega$  are the uptake coefficient and the mean molecular speed of SO<sub>2</sub>, respectively.  $A$  is the surface area density of mineral dust, and it is estimated to be  $(1.4\text{--}4.8) \times 10^{-5} \text{ cm}^2 \text{ cm}^{-3}$  (Zhang et al., 2019; P. He et al., 2018). In this work,  $\gamma_{s,\text{BET}}$  of SO<sub>2</sub> on several mineral oxides was measured to be  $4.39 \times 10^{-7}\text{--}3.45 \times 10^{-5}$  (reaction conditions: SO<sub>2</sub> concentration of 40 ppb, irradiation intensity of  $7.93 \times 10^{16} \text{ photons cm}^{-2} \text{ s}^{-1}$ , and RH of 40 %). Thus, the  $\tau$  of SO<sub>2</sub> with respect to the photooxidation on mineral dust was calculated to be 0.9–240 d, which was shorter than that (54 years) for the photochemical uptake of SO<sub>2</sub> on TiO<sub>2</sub> and the corresponding one (346 d) for the heterogeneous oxidation of SO<sub>2</sub> on ATD in the presence of nitrates (Ma et al., 2019; Zhang et al., 2019). The reaction conditions in this study and those in the literature are different in some respects, and the previously reported SO<sub>2</sub> uptake coefficient ( $10^{-7}\text{--}10^{-6}$ ) had a lower value (Ma et al., 2019). The huge difference in the  $\tau$  of SO<sub>2</sub> was also ascribed to the variation in the surface area density. The content of TiO<sub>2</sub> in mineral dust was only about 1 %. Thus, the surface area density of TiO<sub>2</sub> was about  $10^{-7} \text{ cm}^2 \text{ cm}^{-3}$ , leading to a longer  $\tau$  (54 years) for SO<sub>2</sub> on TiO<sub>2</sub> (Ma et al., 2019). It was comparable to the lifetime (3.6–20 d) of SO<sub>2</sub> for the gas-phase



reaction with •OH at a concentration of  $\sim 10^{-6}$  molec. cm<sup>-3</sup> (Huang et al., 2015; Zhang et al., 2019). Therefore, the photochemical process with the excited state SO<sub>2</sub> acting as a driver on mineral dust was an important pathway for the SO<sub>2</sub> sink in the atmosphere.

Sulfates have a significant influence on the atmosphere, contributing to the haze formation, affecting the activity of aerosols acting as cloud condensation nuclei (CCN) and ice nuclei (IN), and modifying optical property and acidity of aerosols. A sulfate formation rate ( $R$ ) can be obtained using  $\gamma$  in Eq. (8) (Cheng et al., 2016):

$$R = \frac{d[\text{SO}_4^{2-}]}{dt} = \left[ \frac{R_p}{D} + \frac{4}{\gamma\omega} \right]^{-1} A[\text{SO}_2], \quad (8)$$

where  $R_p$  (m) is the radius of mineral dust, which can be estimated using Eq. (9) (Li et al., 2020), which states

$$R_p = (0.254 \times [\text{PM}_{2.5}]/(\mu\text{g m}^{-3}) + 10.259) \times 10^{-9}, \quad (9)$$

where  $[\text{PM}_{2.5}]$  is average PM<sub>2.5</sub> mass concentration and 300  $\mu\text{g m}^{-3}$  is used for the polluted periods in typical China cities (Li et al., 2020; Guo et al., 2014). It was assumed that mineral dust accounted for 50 % of the mass of PM<sub>2.5</sub> (Tohidi et al., 2022), and the mass fraction of SiO<sub>2</sub>, Al<sub>2</sub>O<sub>3</sub>, MgO, and CaO in mineral dust was 60 %, 12.5 %, 4 %, and 6.5 %, respectively (Urupina et al., 2019, 2021; Usher et al., 2003). Thus,  $R$  was determined to be 2.15  $\mu\text{g m}^{-3} \text{h}^{-1}$ . This suggests that the SO<sub>2</sub> uptake on non-photoactive surfaces may be an important sulfate formation pathway under irradiation in some dust-rich conditions.

**Data availability.** The data used in this study are available from the corresponding author upon request (hanch@smm.neu.edu.cn).

**Supplement.** The supplement related to this article is available online at: <https://doi.org/10.5194/acp-24-6757-2024-supplement>.

**Author contributions.** CH, WY, and JM designed and conducted experiments. CH, WY, and JM analyzed the data and prepared the paper with contributions from HY. FL conducted experiments. CH supervised the project.

**Competing interests.** The contact author has declared that none of the authors has any competing interests.

**Disclaimer.** Publisher's note: Copernicus Publications remains neutral with regard to jurisdictional claims made in the text, published maps, institutional affiliations, or any other geographical representation in this paper. While Copernicus Publications makes every effort to include appropriate place names, the final responsibility lies with the authors.

**Financial support.** This research has been supported by the National Natural Science Foundation of China (grant no. 42077198), the LiaoNing Revitalization Talents Program (grant no. XLYC1907185), and the Fundamental Research Funds for the Central Universities (grant nos. N2325034 and N2025011).

**Review statement.** This paper was edited by Thorsten Bartels-Rausch and reviewed by Kangwei Li and two anonymous referees.

## References

- Adams, J. W., Rodriguez, D., and Cox, R. A.: The uptake of SO<sub>2</sub> on Saharan dust: a flow tube study, *Atmos. Chem. Phys.*, 5, 2679–2689, <https://doi.org/10.5194/acp-5-2679-2005>, 2005.
- Alexander, B., Park, R. J., Jacob, D. J., and Gong, S.: Transition metal-catalyzed oxidation of atmospheric sulfur: Global implications for the sulfur budget, *J. Geophys. Res.*, 114, 2309–2312, <https://doi.org/10.1029/2008jd010486>, 2009.
- Ammann, M., Poschl, U., and Rudich, Y.: Effects of reversible adsorption and Langmuir–Hinshelwood surface reactions on gas uptake by atmospheric particles, *Phys. Chem. Chem. Phys.*, 5, 351–356, <https://doi.org/10.1039/b208708a>, 2003.
- Bounechada, D., Anderson, D., Skoglundh, M., and Carlsson, P.: SO<sub>2</sub> adsorption on silica supported iridium, *J. Chem. Phys.*, 146, 084701–084708, <https://doi.org/10.1063/1.4976835>, 2017.
- Brunauer, B., Deming, L., Deming, W., and Teller, E.: Adsorption of gases in multimolecular layers, *J. Am. Chem. Soc.*, 60, 309–319, <https://doi.org/10.1021/ja01269a023>, 1938.
- Bulgakov, R. G. and Safonova, L. A.: Chemiluminescence in the oxidation of Na<sub>2</sub>S by oxygen in water solutions, *Russ. Chem. B.*, 45, 1775–1776, <https://doi.org/10.1007/bf01431827>, 1996.
- Cao, J., Tie, X., Dabberdt, W. F., Jie, T., Zhao, Z., An, Z., Shen, Z., and Feng, Y.: On the potential high acid deposition in northeastern China, *J. Geophys. Res.-Atmos.*, 118, 4834–4846, <https://doi.org/10.1002/jgrd.50381>, 2013.
- Chan, M. and Chan, C.: Hygroscopic properties of two model humic-like substances and their mixtures with inorganics of atmospheric importance, *Environ. Sci. Technol.*, 37, 5109–5115, <https://doi.org/10.1021/es034272o>, 2003.
- Chen, Y., Tong, S., Li, W., Liu, Y., Tan, F., Ge, M., Xie, X., and Sun, J.: Photocatalytic oxidation of SO<sub>2</sub> by TiO<sub>2</sub>: Aerosol formation and the key role of gaseous reactive oxygen species, *Environ. Sci. Technol.*, 55, 9784–9793, <https://doi.org/10.1021/acs.est.1c01608>, 2021.
- Cheng, Y., Zheng, G., Wei, C., Mu, Q., Zheng, B., Wang, Z., Gao, M., Zhang, Q., He, K., Carmichael, G., Pöschl, U., and Su, H.: Reactive nitrogen chemistry in aerosol water as a source of sulfate during haze events in China, *Sci. Adv.*, 2, 1601530–1601540, <https://doi.org/10.1126/sciadv.1601530>, 2016.
- Chu, B., Wang, Y., Yang, W., Ma, J., Ma, Q., Zhang, P., Liu, Y., and He, H.: Effects of NO<sub>2</sub> and C<sub>3</sub>H<sub>6</sub> on the heterogeneous oxidation of SO<sub>2</sub> on TiO<sub>2</sub> in the presence or absence of UV–Vis irradiation, *Atmos. Chem. Phys.*, 19, 14777–14790, <https://doi.org/10.5194/acp-19-14777-2019>, 2019.
- Davis, D. D., Ravishankara, A. R., and Fischer, S.: SO<sub>2</sub> oxidation via the hydroxyl radical: Atmospheric fate

- of HSO<sub>x</sub> radicals, *Geophys. Res. Lett.*, 6, 113–116, <https://doi.org/10.1029/GL006i002p00113>, 1979.
- Dentener, F., Carmichael, G., Zhang, Y., Lelieveld, J., and Crutzen, P.: Role of mineral aerosol as a reactive surface in the global troposphere, *J. Geophys. Res.-Atmos.*, 101, 22869–22889, <https://doi.org/10.1029/96jd01818>, 1996.
- Gen, M., Zhang, R., Huang, D., Li, Y., and Chan, C.: Heterogeneous oxidation of SO<sub>2</sub> in sulfate production during nitrate photolysis at 300 nm: Effect of pH, relative humidity, irradiation intensity, and the presence of organic compounds, *Environ. Sci. Technol.*, 53, 8757–8766, <https://doi.org/10.1021/acs.est.9b01623>, 2019a.
- Gen, M., Zhang, R., Huang, D., Li, Y., and Chan, C.: Heterogeneous SO<sub>2</sub> oxidation in sulfate formation by photolysis of particulate nitrate, *Environ. Sci. Technol.*, 6, 86–91, <https://doi.org/10.1021/acs.estlett.8b00681>, 2019b.
- Golobokova, L., Khodzher, T., Khuriganova, O., Marinayte, I., Onishchuk, N., Rusanova, P., and Potemkin, V.: Variability of chemical properties of the atmospheric aerosol above lake baikal during large wildfires in siberia, *Atmosphere*, 11, 1230–1250, <https://doi.org/10.3390/atmos11111230>, 2020.
- Gong, C., Yuan, X., Xing, D., Zhang, D., Martins-Costa, M. T. C., Anglada, J. M., Ruiz-Lopez, M. F., Francisco, J. S., and Zhang, X.: Fast sulfate formation initiated by the spin-forbidden excitation of SO<sub>2</sub> at the air-water interface, *J. Am. Chem. Soc.*, 144, 22302–22308, <https://doi.org/10.1021/jacs.2c10830>, 2022.
- Goodman, A., Li, P., Usher, C., and Grassian, V.: Heterogeneous uptake of sulfur dioxide on aluminum and magnesium oxide particles, *J. Phys. Chem. A*, 105, 6109–6120, <https://doi.org/10.1021/jp004423z>, 2001.
- Guo, S., Hu, M., Zamora, M. L., Peng, J., Shang, D., Zheng, J., Du, Z., Wu, Z., Shao, M., Zeng, L., Molina, M. J., and Zhang, R.: Elucidating severe urban haze formation in China, *P. Natl. Acad. Sci. USA*, 111, 17373–17378, <https://doi.org/10.1073/pnas.1419604111>, 2014.
- Harris, E., Sinha, B., van Pinxteren, D., Tilgner, A., Fomba, K. W., Schneider, J., Roth, A., Gnauk, T., Fahlbusch, B., Mertes, S., Lee, T., Collett, J., Foley, S., Borrmann, S., Hoppe, P., and Herrmann, H.: Enhanced role of transition metal ion catalysis during in-cloud oxidation of SO<sub>2</sub>, *Science*, 340, 727–730, <https://doi.org/10.1126/science.1230911>, 2013.
- He, G., Ma, J., and He, H.: Role of carbonaceous aerosols in catalyzing sulfate formation, *ACS Catal.*, 8, 3825–3832, <https://doi.org/10.1021/acscatal.7b04195>, 2018.
- He, H., Li, C., Loughner, C. P., Li, Z., Krotkov, N. A., Yang, K., Wang, L., Zheng, Y., Bao, X., Zhao, G., and Dickerson, R. R.: SO<sub>2</sub> over central China: Measurements, numerical simulations and the tropospheric sulfur budget, *J. Geophys. Res.-Atmos.*, 117, 37–51, <https://doi.org/10.1029/2011jd016473>, 2012.
- He, P., Alexander, B., Geng, L., Chi, X., Fan, S., Zhan, H., Kang, H., Zheng, G., Cheng, Y., Su, H., Liu, C., and Xie, Z.: Isotopic constraints on heterogeneous sulfate production in Beijing haze, *Atmos. Chem. Phys.*, 18, 5515–5528, <https://doi.org/10.5194/acp-18-5515-2018>, 2018.
- Herrmann, H., Ervens, B., Jacobi, H. W., Wolke, R., Nowacki, P., and Zellner, R.: CAPRAM<sub>2.3</sub>: A chemical aqueous phase radical mechanism for tropospheric chemistry, *J. Atmos. Chem.*, 36, 231–284, <https://doi.org/10.1023/A:1006318622743>, 2000.
- Hu, Q., Suzuki, H., Gao, H., Araki, H., Yang, W., and Noda, T.: High-frequency FTIR absorption of SiO<sub>2</sub>/Si nanowires, *Chem. Phys. Lett.*, 378, 299–304, <https://doi.org/10.1016/j.cplett.2003.07.015>, 2003.
- Huang, L., Zhao, Y., Li, H., and Chen, Z.: Kinetics of heterogeneous reaction of sulfur dioxide on authentic mineral dust: Effects of relative humidity and hydrogen peroxide, *Environ. Sci. Technol.*, 49, 10797–10805, <https://doi.org/10.1021/acs.est.5b03930>, 2015.
- Knopf, D., Cosman, L., Mousavi, P., Mokamati, S., and Bertram, A.: A novel flow reactor for studying reactions on liquid surfaces coated by organic monolayers: Methods, validation, and initial results, *J. Phys. Chem. A*, 111, 11021–11032, <https://doi.org/10.1021/jp075724c>, 2007.
- Kroll, J., Frandsen, B., Kjaergaard, H., and Vaida, V.: Atmospheric hydroxyl radical source: Reaction of triplet SO<sub>2</sub> and water, *J. Phys. Chem. A*, 122, 4465–4469, <https://doi.org/10.1021/acs.jpca.8b03524>, 2018.
- Langhammer, D., Kullgren, J., and Osterlund, L.: Photoinduced adsorption and oxidation of SO<sub>2</sub> on anatase TiO<sub>2</sub>, *J. Am. Chem. Soc.*, 142, 21767–21774, <https://doi.org/10.1021/jacs.0c09683>, 2020.
- Li, G., Bei, N., Cao, J., Huang, R., Wu, J., Feng, T., Wang, Y., Liu, S., Zhang, Q., Tie, X., and Molina, L. T.: A possible pathway for rapid growth of sulfate during haze days in China, *Atmos. Chem. Phys.*, 17, 3301–3316, <https://doi.org/10.5194/acp-17-3301-2017>, 2017.
- Li, J., Zhang, Y. L., Cao, F., Zhang, W., Fan, M., Lee, X., and Michalski, G.: Stable sulfur isotopes revealed a major role of transition-metal ion-catalyzed SO<sub>2</sub> oxidation in haze episodes, *Environ. Sci. Technol.*, 54, 2626–2634, <https://doi.org/10.1021/acs.est.9b07150>, 2020.
- Li, K., Kong, L., Zhanzakova, A., Tong, S., Shen, J., Wang, T., Chen, L., Li, Q., Fu, H., and Zhang, L.: Heterogeneous conversion of SO<sub>2</sub> on nano α-Fe<sub>2</sub>O<sub>3</sub>: the effects of morphology, light illumination and relative humidity, *Environ. Sci.: Nano*, 6, 1838–1851, <https://doi.org/10.1039/c9en00097f>, 2019.
- Lim, S., Lee, M., Kim, S., and Laj, P.: Sulfate alters aerosol absorption properties in East Asian outflow, *Sci. Rep.-UK*, 8, 5172–5178, <https://doi.org/10.1038/s41598-018-23021-1>, 2018.
- Liu, T., Clegg, S., and Abbatt, J. P. D.: Fast oxidation of sulfur dioxide by hydrogen peroxide in deliquesced aerosol particles, *P. Natl. Acad. Sci. USA*, 117, 1354–1359, <https://doi.org/10.1073/pnas.1916401117>, 2020.
- Liu, T., Chan, A. W. H., and Abbatt, J. P. D.: Multiphase oxidation of sulfur dioxide in aerosol particles: Implications for sulfate formation in polluted environments, *Environ. Sci. Technol.*, 55, 4227–4242, <https://doi.org/10.1021/acs.est.0c06496>, 2021.
- Liu, Y., Deng, Y., Liu, J., Fang, X., Wang, T., Li, K., Gong, K., Bacha, A. U., Nabi, I., Ge, Q., Zhang, X., George, C., and Zhang, L.: A novel pathway of atmospheric sulfate formation through carbonate radicals, *Atmos. Chem. Phys.*, 22, 9175–9197, <https://doi.org/10.5194/acp-22-9175-2022>, 2022.
- Ma, J., Dörner, S., Donner, S., Jin, J., Cheng, S., Guo, J., Zhang, Z., Wang, J., Liu, P., Zhang, G., Pukite, J., Lampel, J., and Wagner, T.: MAX-DOAS measurements of NO<sub>2</sub>, SO<sub>2</sub>, HCHO, and BrO at the Mt. Waliguan WMO GAW global baseline station in the Tibetan Plateau, *Atmos. Chem. Phys.*, 20, 6973–6990, <https://doi.org/10.5194/acp-20-6973-2020>, 2020.
- Ma, Q., Wang, L., Chu, B., Ma, J., and He, H.: Contrary role of H<sub>2</sub>O and O<sub>2</sub> in the kinetics of heterogeneous photochemical re-

- actions of SO<sub>2</sub> on TiO<sub>2</sub>, *J. Phys. Chem. A*, 123, 1311–1318, <https://doi.org/10.1021/acs.jpca.8b11433>, 2019.
- Martins-Costa, M., Anglada, J., Francisco, J., and Ruiz-Lopez, M.: Photochemistry of SO<sub>2</sub> at the air-water interface: A source of OH and HOSO radicals, *J. Am. Chem. Soc.*, 140, 12341–12344, <https://doi.org/10.1021/jacs.8b07845>, 2018.
- Mauldin, R., Berndt, T., Sipila, M., Paasonen, P., Petaja, T., Kim, S., Kurten, T., Stratmann, F., Kerminen, V., and Kulmala, M.: A new atmospherically relevant oxidant of sulphur dioxide, *Nature*, 488, 193–196, <https://doi.org/10.1038/nature11278>, 2012.
- Mukuta, T., Fukazawa, N., Murata, K., Inagaki, A., Akita, M., Tanaka, S., Koshihara, S. Y., and Onda, K.: Infrared vibrational spectroscopy of [Ru(bpy)<sub>2</sub>(bpm)]<sup>2+</sup> and [Ru(bpy)<sub>3</sub>]<sup>2+</sup> in the excited triplet state, *Inorg. Chem.*, 53, 2481–2490, <https://doi.org/10.1021/ic402474t>, 2014.
- Olson, E., Michalski, G., Welp, L., Valdivia, A., Larico, J., Pen, J., Fang, H., Gomez, K., and Li, J.: Mineral dust and fossil fuel combustion dominate sources of aerosol sulfate in urban Peru identified by sulfur stable isotopes and water-soluble ions, *Atmos. Environ.*, 260, 118482–118495, <https://doi.org/10.1016/j.atmosenv.2021.118482>, 2021.
- Park, J. and Jang, M.: Heterogeneous photooxidation of sulfur dioxide in the presence of airborne mineral dust particles, *RSC Adv.*, 6, 58617–58627, <https://doi.org/10.1039/c6ra09601h>, 2016.
- Park, J., Jang, M., and Yu, Z.: Heterogeneous photo-oxidation of SO<sub>2</sub> in the presence of two different mineral dust particles: Gobi and arizona dust, *Environ. Sci. Technol.*, 51, 9605–9613, <https://doi.org/10.1021/acs.est.7b00588>, 2017.
- Peng, Y., von Salzen, K., and Li, J.: Simulation of mineral dust aerosol with Piecewise Log-normal Approximation (PLA) in CanAM4-PAM, *Atmos. Chem. Phys.*, 12, 6891–6914, <https://doi.org/10.5194/acp-12-6891-2012>, 2012.
- Prospero, J.: Long-range transport of mineral dust in the global atmosphere: Impact of African dust on the environment of the southeastern United States, *P. Natl. Acad. Sci. USA*, 96, 3396–3403, <https://doi.org/10.1073/pnas.96.7.3396>, 1999.
- Shao, J., Chen, Q., Wang, Y., Lu, X., He, P., Sun, Y., Shah, V., Martin, R. V., Philip, S., Song, S., Zhao, Y., Xie, Z., Zhang, L., and Alexander, B.: Heterogeneous sulfate aerosol formation mechanisms during wintertime Chinese haze events: air quality model assessment using observations of sulfate oxygen isotopes in Beijing, *Atmos. Chem. Phys.*, 19, 6107–6123, <https://doi.org/10.5194/acp-19-6107-2019>, 2019.
- Shiraiwa, M., Ueda, K., Pozzer, A., Lammel, G., Kampf, C. J., Fushimi, A., Enami, S., Arangio, A. M., Frohlich-Nowoisky, J., Fujitani, Y., Furuyama, A., Lakey, P. S. J., Lelieveld, J., Lucas, K., Morino, Y., Poschl, U., Takahama, S., Takami, A., Tong, H., Weber, B., Yoshino, A., and Sato, K.: Aerosol health effects from molecular to global scales, *Environ. Sci. Technol.*, 51, 13545–13567, <https://doi.org/10.1021/acs.est.7b04417>, 2017.
- Sidebottom, H. W., Badcock, C. C., Jackson, G. E., Calvert, J. G., Reinhardt, G. W., and Damon, E. K.: Photooxidation of sulfur dioxide, *Environ. Sci. Technol.*, 6, 72–79, <https://doi.org/10.1080/00022470.1971.10469552>, 1972.
- Solbrig, C. W. and Gidaspow, D.: Convective diffusion in a parallel plate duct with one catalytic wall, laminar flow, first-order reaction-part one, *Can. J. Chem. Eng.*, 45, 35–39, [https://doi.org/10.1016/0304-5102\(89\)80197-X](https://doi.org/10.1016/0304-5102(89)80197-X), 1967.
- Sumner, A. L., Menke, E. J., Dubowski, Y., Newberg, J. T., Penner, R. M., Hemminger, J. C., Wingen, L. M., Brauers, T., and Finlayson-Pitts, B. J.: The nature of water on surfaces of laboratory systems and implications for heterogeneous chemistry in the troposphere, *Phys. Chem. Chem. Phys.*, 6, 604–613, <https://doi.org/10.1039/B308125G>, 2004.
- Tohidi, R., Farahani, V., and Sioutas, C.: Real-time measurements of mineral dust concentration in coarse particulate matter PM<sub>10-2.5</sub> by employing a novel optical-based technique in Los Angeles, *Sci. Total Environ.*, 838, 156215–156226, <https://doi.org/10.1016/j.scitotenv.2022.156215>, 2022.
- Urupina, D., Lasne, J., Romanias, M. N., Thiery, V., Dagsson-Waldhauserova, P., and Thevenet, F.: Uptake and surface chemistry of SO<sub>2</sub> on natural volcanic dusts, *Atmos. Environ.*, 217, 116942–116959, <https://doi.org/10.1016/j.atmosenv.2019.116942>, 2019.
- Urupina, D., Romanias, M. N., and Thevenet, F.: How relevant is it to use mineral proxies to mimic the atmospheric reactivity of natural dust samples? A reactivity study using SO<sub>2</sub> as probe molecule, *Minerals*, 11, 282–299, <https://doi.org/10.3390/min11030282>, 2021.
- Usher, C., Al-Hosney, H., Carlos-Cuellar, S., and Grassian, V.: A laboratory study of the heterogeneous uptake and oxidation of sulfur dioxide on mineral dust particles, *J. Geophys. Res.-Atmos.*, 107, 4713–4729, <https://doi.org/10.1029/2002jd002051>, 2002.
- Usher, C., Michel, A., and Grassian, V.: Reactions on mineral dust, *Chem. Rev.*, 103, 4883–4939, <https://doi.org/10.1021/cr020657y>, 2003.
- Wang, J., Li, J., Ye, J., Zhao, J., Wu, Y., Hu, J., Liu, D., Nie, D., Shen, F., Huang, X., Huang, D. D., Ji, D., Sun, X., Xu, W., Guo, J., Song, S., Qin, Y., Liu, P., Turner, J. R., Lee, H. C., Hwang, S., Liao, H., Martin, S. T., Zhang, Q., Chen, M., Sun, Y., Ge, X., and Jacob, D. J.: Fast sulfate formation from oxidation of SO<sub>2</sub> by NO<sub>2</sub> and HONO observed in Beijing haze, *Nat. Commun.*, 11, 2844–2850, <https://doi.org/10.1038/s41467-020-16683-x>, 2020.
- Wang, S., Zhou, S., Tao, Y., Tsui, W. G., Ye, J., Yu, J. Z., Murphy, J. G., McNeill, V. F., Abbatt, J. P. D., and Chan, A. W. H.: Organic peroxides and sulfur dioxide in aerosol: Source of particulate sulfate. *Environ. Sci. Technol.*, 53, 10695–10704, <https://doi.org/10.1021/acs.est.9b02591>, 2019.
- Wang, T., Liu, Y., Deng, Y., Fu, H., Zhang, L., and Chen, J.: The influence of temperature on the heterogeneous uptake of SO<sub>2</sub> on hematite particles, *Sci. Total Environ.*, 644, 1493–1502, <https://doi.org/10.1016/j.scitotenv.2018.07.046>, 2018.
- Wang, T., Liu, Y. Y., Deng, Y., Cheng, H. Y., Yang, Y., Li, K. J., Fang, X. Z., and Zhang, L. W.: Irradiation intensity dependent heterogeneous formation of sulfate and dissolution of ZnO nanoparticles, *Environ. Sci.: Nano*, 7, 327–338, <https://doi.org/10.1039/c9en01148j>, 2020.
- Wang, Z., Wang, T., Fu, H., Zhang, L., Tang, M., George, C., Grassian, V. H., and Chen, J.: Enhanced heterogeneous uptake of sulfur dioxide on mineral particles through modification of iron speciation during simulated cloud processing, *Atmos. Chem. Phys.*, 19, 12569–12585, <https://doi.org/10.5194/acp-19-12569-2019>, 2019.
- Xu, M., Qiu, P., He, Y., Guo, S., Bai, Y., Zhang, H., Zhao, S., Shen X., Zhu, B., Guo, Q., Guo, Z., Sulfur isotope composition during heterogeneous oxidation of SO<sub>2</sub> on mineral dust: The effect of

- temperature, relative humidity, and light intensity, *Atmos. Res.*, 254, 105513, <https://doi.org/10.1016/j.atmosres.2021.105513>, 2021.
- Yang, N., Tsona, N. T., Cheng, S., Li, S., Xu, L., Wang, Y., Wu, L., and Du, L.: Competitive reactions of SO<sub>2</sub> and acetic acid on  $\alpha$ -Al<sub>2</sub>O<sub>3</sub> and CaCO<sub>3</sub> particles, *Sci. Total Environ.*, 699, 134362–134370, <https://doi.org/10.1016/j.scitotenv.2019.134362>, 2020.
- Yang, W., Ma, Q., Liu, Y., Ma, J., Chu, B., and He, H.: The effect of water on the heterogeneous reactions of SO<sub>2</sub> and NH<sub>3</sub> on the surfaces of  $\alpha$ -Fe<sub>2</sub>O<sub>3</sub> and  $\alpha$ -Al<sub>2</sub>O<sub>3</sub>, *Environ. Sci.: Nano*, 6, 2749–2758, <https://doi.org/10.1039/c9en00574a>, 2019.
- Yao, M., Zhao, Y., Hu, M., Huang, D., Wang, Y., Yu, J. Z., and Yan, N.: Multiphase reactions between secondary organic aerosol and sulfur dioxide: Kinetics and contributions to sulfate formation and aerosol aging. *Environ. Sci. Technol. Lett.*, 6, 768–774, <https://doi.org/10.1021/acs.estlett.9b00657>, 2019.
- Ye, J., Abbatt, J. P. D., and Chan, A. W. H.: Novel pathway of SO<sub>2</sub> oxidation in the atmosphere: reactions with monoterpene ozonolysis intermediates and secondary organic aerosol, *Atmos. Chem. Phys.*, 18, 5549–5565, <https://doi.org/10.5194/acp-18-5549-2018>, 2018.
- Zhang, P., Chen, T., Ma, Q., Chu, B., Wang, Y., Mu, Y., Yu, Y., and He, H.: Diesel soot photooxidation enhances the heterogeneous formation of H<sub>2</sub>SO<sub>4</sub>, *Nat. Commun.*, 13, 5364–5372, <https://doi.org/10.1038/s41467-022-33120-3>, 2022.
- Zhang, R., Gen, M., Huang, D., Li, Y., and Chan, C.: Enhanced sulfate production by nitrate photolysis in the presence of halide ions in atmospheric particles, *Environ. Sci. Technol.*, 54, 3831–3839, <https://doi.org/10.1021/acs.est.9b06445>, 2020.
- Zhang, T., Yang, W., Han, C., Yang, H., and Xue, X.: Heterogeneous reaction of ozone with syringic acid: Uptake of O<sub>3</sub> and changes in the composition and optical property of syringic acid, *Environ. Pollut.*, 257, 113632–113638, <https://doi.org/10.1016/j.envpol.2019.113632>, 2020.
- Zhang, X., Zhuang, G., Chen, J., Wang, Y., Wang, X., An, Z., and Zhang, P.: Heterogeneous reactions of sulfur dioxide on typical mineral particles, *J. Phys. Chem. B*, 110, 12588–12596, <https://doi.org/10.1021/jp0617773>, 2006.
- Zhang, Y., Bao, F., Li, M., Chen, C., and Zhao, J.: Nitrate-enhanced oxidation of SO<sub>2</sub> on mineral dust: A vital role of a proton, *Environ. Sci. Technol.*, 53, 10139–10145, <https://doi.org/10.1021/acs.est.9b01921>, 2019.
- Zhang, Y., Bao, F., Li, M., Xia, H., Huang, D., Chen, C., and Zhao, J.: Photoinduced uptake and oxidation of SO<sub>2</sub> on Beijing urban PM<sub>2.5</sub>, *Environ. Sci. Technol.*, 54, 14868–14876, <https://doi.org/10.1021/acs.est.0c01532>, 2020.